

Output analysis of sandwiched two-layer arrays for cancellation of zeroth order

WEIYI YU, BO WANG*, HONG ZOU, JIAHAO LI, XIAOFENG WANG, JINHAI HUANG, LIQUN LIU, LINJIAN HUANG, XU YANG, GUODING CHEN, LIANG LEI, QU WANG

School of Physics and Optoelectronic Engineering, Guangdong University of Technology, Guangzhou 510006, China

In this paper, a sandwich structure two-port transmission beam splitter with two-layer array is proposed. By using rigorous coupled-wave analysis and simulated annealing algorithm, the structure and parameters of the grating are analyzed and optimized to achieve high efficiency diffraction and zero order suppression. At normal incidence of 800 nm incident light, the diffraction efficiency of the grating at ± 1 st transverse magnetic polarization and transverse polarization is 48.83% and 49.12% respectively. In addition, the grating can still maintain high efficiency within the process tolerance range of some parameters (including incident wavelength, duty cycle, incident angle and grating period).

(Received November 16, 2022; accepted June 6, 2023)

Keywords: Sandwiched two-layer arrays, Cancellation of zeroth order, Simulated annealing

1. Introduction

Beam splitter is one of the indispensable devices in the field of optoelectronics [1-3]. It can split the original incident beam into multiple beams with different propagation angles and powers but the same optical characteristics. With the development of modern science and technology, the realization of micro-nano and integrated optical devices has gradually become the goal pursued by researchers in the optical field. Therefore, the traditional beam splitter is being replaced by polarization-independent micro-nano gratings [4,5]. Because of its small size, easy integration and high efficiency, it is widely used in optical sensing [6-10], photoelectric detection [11-13], coupler [14-17] and other fields. Xiong et al. proposed a two-port reflective grating based on a two-layer array and a metal film structure. Under the normal incidence of the incident light with the wavelength of 1550 nm, for TE and TM polarization, the reflection efficiency of ± 1 st is 48.07% and 47.40%, respectively, and the reflection efficiency of 0th is almost completely suppressed [18]. Zhu et al. designed a two-port transmission grating based on a double dielectric rectangular slot. Under normal incidence, the diffraction efficiency of ± 1 st of the grating under TE and TM polarization is 47.62% and 47.26% respectively [19].

At present, scalar diffraction theory and vector diffraction theory are two main theories to study the diffraction characteristics of optical devices. For subwavelength gratings, their polarization characteristics are particularly obvious. When the grating period is close to the wavelength, the scalar diffraction theory will lack reliability. In order to accurately analyze its diffraction

characteristics, the grating should be analyzed by vector diffraction theory, including modal method, rigorous coupled-wave analysis (RCWA) [20-22], finite element method (FEM) [23-26] and finite difference time domain method and so on. Among various numerical methods, RCWA has become one of the most widely used methods to analyze the characteristics of subwavelength gratings due to its excellent computational efficiency. Modal method is another different theoretical approach to design and explain grating compared with the numerical RCWA, which describes the physical process of grating diffraction. For low contrast deep etching gratings, the influence of reflection and evanescent grating modes at the interface can be ignored, so the simplified mode method (SMM) [27-29] is introduced. When considering the symmetry of grating modes, SMM can give approximate analytical expressions to calculate the diffraction efficiency of these gratings under Littrow incidence. These expressions can be used to solve the anti-grating problem and are very helpful for the design of beam splitting gratings.

In this paper, an efficient two-port transmission beam splitter based on two-layer array sandwich gratings is introduced. By using rigorous coupled-wave analysis (RCWA) and simulated annealing (SA) [30-34] algorithm to analyze and optimize the structure and parameters of the splitter, not only the high efficiency of TE and TM polarization is achieved, but also almost completely suppresses the zero order diffraction efficiency. The results show that the total transmission efficiency of ± 1 st is more than 98% for TE and TM polarization, and the transmission efficiency of 0th is less than 1.5% under the normal incidence of 800 nm wavelength. In addition, this paper uses FEM to verify the accuracy of the research

results. Through analysis, it is found that the period, incident angle and duty cycle of the grating can still maintain high efficiency within a certain tolerance range, and also has the characteristics of wide bandwidth (63 nm bandwidth). Therefore, as an optical element with stable optical characteristics and high efficiency, its application in the optical field is worth looking forward to.

2. Structural analysis and parameter calculation

Fig. 1 shows the two-dimensional and three-dimensional structure diagrams of the two-layer array sandwich gratings respectively. As can be seen from Fig. 1, the grating consists of a covering layer, a grating

layer (including grating ridge and grating groove) and a substrate. The grating ridge is divided into two layers. The upper layer is Al_2O_3 layer with thickness of h_1 and refractive index of $n_3=1.76$, and the lower layer is TiO_2 layer with thickness of h_2 and refractive index of $n_2=2.59$. The covering layer and the substrate are composed of fused quartz layers with a refractive index of $n_4=1.45$. Adding fused quartz layer as the covering layer on the single-layer structure grating can protect the grating layer to a certain extent, prolong the service life of the grating and save costs in practical applications. The thickness of grating groove is h_1+h_2 , and the material used is air with refractive index $n_1=1.00$. In addition, b and d represent the width of grating ridge and grating period respectively, and the duty cycle is defined as $f=b/d$.

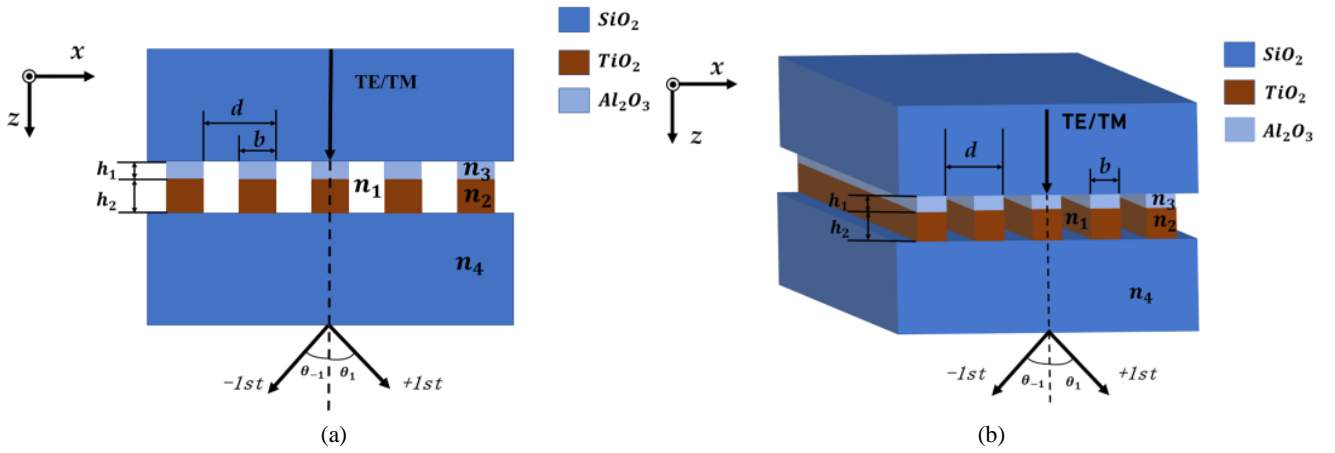


Fig. 1. The (a) two-dimensional and (b) three-dimensional schematic diagram of beam splitter gratings with double-layer array sandwich structure under normal incidence (color online)

Rigorous coupled-wave analysis is widely used in the analysis and design of various types of gratings, which is a direct and effective electromagnetic theory. By strictly solving Maxwell's equations in the grating region and solving the boundary conditions on the interface between the grating region and other regions, the diffraction efficiency of each diffraction order can be finally calculated. In this study, because the incident light is normal incidence and $\pm 1st$ has symmetry, only the diffraction efficiency of TE and TM polarization at the 1st needs to be considered. The following processes can be derived from RCWA:

$$\eta_i = R_i R_i^* \text{Re} \left(\frac{k_{I,zi}}{n_1 k_0 \cos \theta} \right), \quad (1)$$

where R_i represents the complex amplitude of normalized electric field amplitude and normalized magnetic field amplitude under TE and TM polarization respectively. η_i is the diffraction efficiency of the i -th order with

$$k_{I,zi} = \begin{cases} +k_0 \sqrt{n_I^2 - \left(\frac{k_{xi}}{k_0}\right)^2}, & k_0 n_I > k_{xi} \\ -jk_0 \sqrt{\left(\frac{k_{xi}}{k_0}\right)^2 - n_I^2}, & k_0 n_I < k_{xi} \end{cases}, \quad (2)$$

where $k_0 = 2\pi/\lambda$ represents the wave vector of incident light in vacuum, k_{xi} represents the wave vector component of the i -order diffracted wave in the x -direction, which can be obtained from Floquet condition:

$$k_{xi} = k_0 [n_I \sin \theta - i(\lambda/d)]. \quad (3)$$

Simulated annealing (SA) algorithm is a general optimization algorithm. Theoretically, the algorithm has the global optimization performance of probability. Combined with the jumping characteristics of probability, it can randomly find the global optimal solution of the objective function in the solution space. In order to quickly and conveniently optimize the grating period d , the thickness of the grating ridge h_1 and h_2 , and the duty

cycle f , and find the optimal parameters of the grating, we can set the grating period d between one and two times the wavelength to achieve three levels of diffraction, and then introduce the target function of SA:

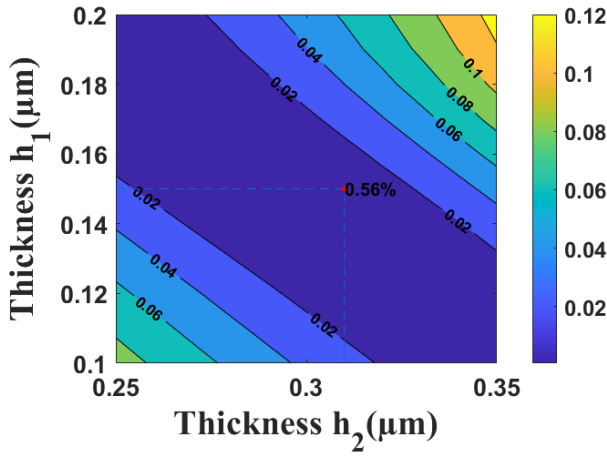
$$\varphi(d, f, h_1, h_2) = \sum_{\lambda} [(1 - 2DE_{TE(1)})^2 + (1 - 2DE_{TM(1)})^2], \quad (4)$$

where $DE_{TE(1)}$ and $DE_{TM(1)}$ represents the diffraction efficiency of TE polarization and TM polarization at 1st, respectively. The optimal parameters of grating structure obtained through numerical calculation are listed in Table 1, which are respectively $h_1=0.15 \mu\text{m}$, $h_2=0.31 \mu\text{m}$, $f=0.38$ and $d=1007 \text{ nm}$. Fig. 2 is a series of contour maps drawn based on the above parameters to describe the

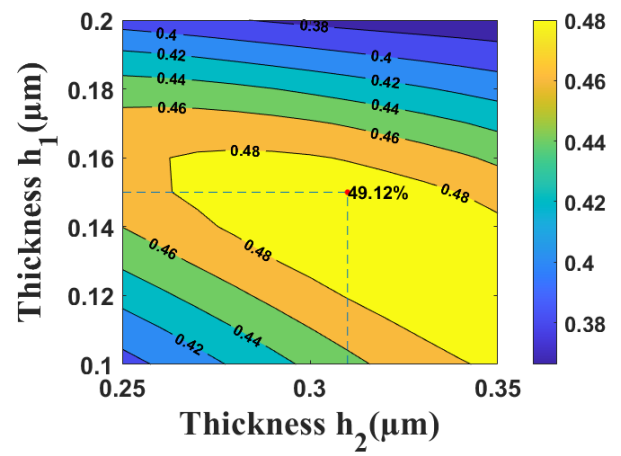
relationship between thickness h_1 , h_2 and transmission efficiency. From the contour maps, it can be clearly seen when $h_1=0.15 \mu\text{m}$ and $h_2=0.31 \mu\text{m}$, for TE polarization, the efficiency of $\pm 1\text{st}$ reaches 49.12%, and the diffraction efficiency of 0th is almost completely suppressed, only 0.56%. For TM polarization, the diffraction efficiency of $\pm 1\text{st}$ is 48.83%, and that of 0th is 1.38%.

Table 1. The optimum parameters of the beam splitter with double-layer array sandwich structure

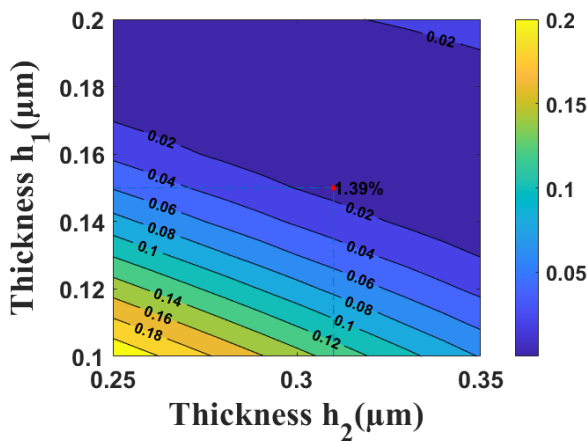
F	D	h_1	h_2
0.38	1.007 μm	0.15 μm	0.31 μm



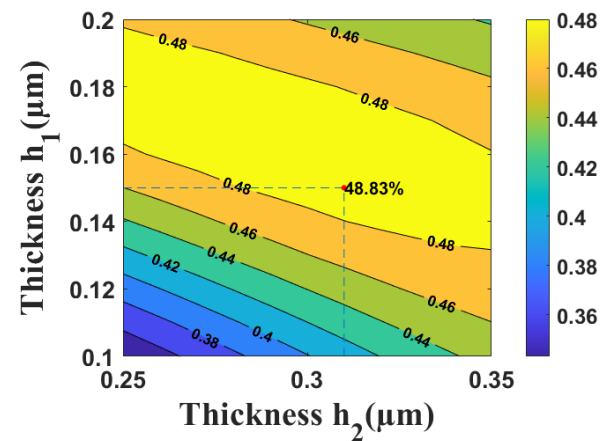
(a)



(b)



(c)



(d)

Fig. 2. The contour map of the relationship between reflective efficiencies and the depths of h_1 and h_2 for TE polarization and TM polarization with incident wavelength $\lambda=800 \text{ nm}$, period $d=1007 \text{ nm}$, duty cycle $f=0.38$ under normal incidence: (a) 0th order for TE polarization, (b) $\pm 1\text{st}$ orders for TE polarization, (c) 0th order for TM polarization, (d) $\pm 1\text{st}$ orders for TM polarization (color online)

3. Analysis and discussions

By analyzing the normalized electric field distribution of the grating, we can clearly see the physical process and energy distribution of the incident light entering the grating. Fig. 3 shows the normalized electric field distribution of two-port transmission gratings with two-layer array sandwich structure under TE and TM polarization respectively. The incident light is normally incident in the SiO_2 covering layer, passes through two layers of grating ridges in the grating layer, and finally

emits from the SiO_2 substrate. It can be seen from the figures that the structure of the grating is periodic, so the internal energy distribution also shows a periodic law. For TE polarization, most of the incident light energy is concentrated in the TiO_2 layer of the grating ridge, and there is a small part of energy distribution at the junction of two grating ridges and the edge of the upper grating ridge; for TM polarization, the maximum energy is almost completely distributed in TiO_2 layer, and there is basically no energy distribution in Al_2O_3 layer.

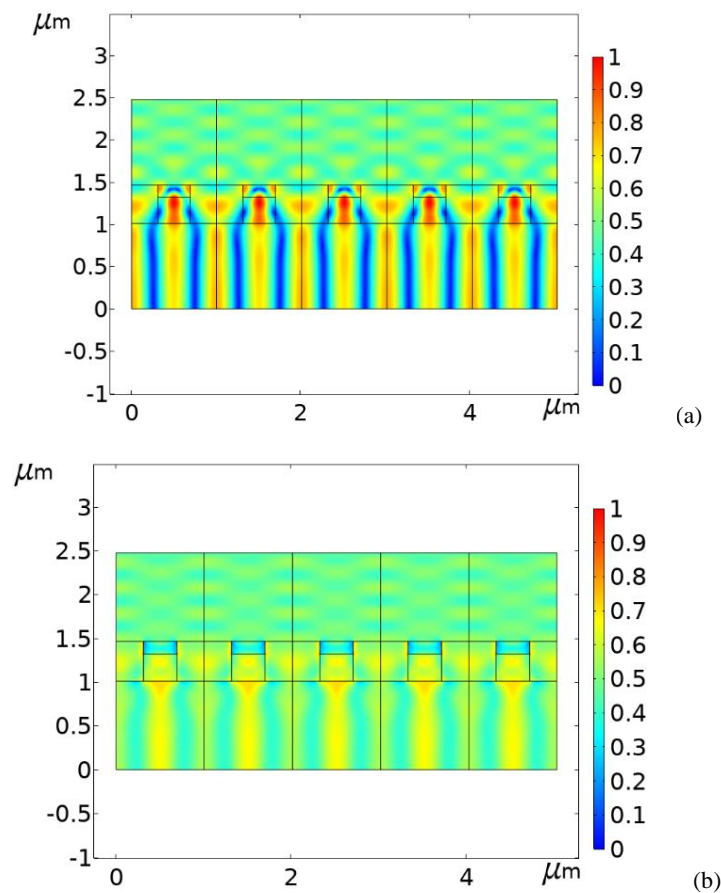


Fig. 3. Distribution of normalized electric field of sandwich grating under normal incidence: (a) TE polarization (b) TM polarization (color online)

In order to verify the accuracy of the calculation results and ensure that the parameters obtained under this structure are the optimal parameters. Based on the grating parameters obtained by RCWA, we use FEM to calculate the diffraction efficiency of TE and TM polarization of grating at 0th and ± 1 st, and list the results obtained by FEM and RCWA in Table 2. Through data comparison, it can be found that the diffraction efficiency calculated by the two methods is almost the same, which effectively proves that the grating parameters are optimal and accurate.

Table 2. The transmission efficiencies of the grating obtained by FEM and RCWA for TE polarization and TM polarization with period $d = 1007$ nm, incident wavelength $\lambda = 800$ nm, duty cycle $f = 0.38$, $h_1 = 0.15$ μm , $h_2 = 0.31$ μm

Theory	$\eta_{\pm 1}^{\text{TE}}$ (%)	$\eta_{\pm 1}^{\text{TM}}$ (%)	η_0^{TE} (%)	η_0^{TM} (%)
RCWA	49.12	48.83	0.56	1.40
FEM	49.12	48.83	0.57	1.39

For subwavelength metal gratings, many parameters, such as metal material, grating period, incident angle, duty cycle and incident wavelength, will affect the performance of gratings. Because in the actual manufacturing process of grating, due to the influence of manufacturing process and technology, some parameters often have slight deviation, which affects the performance of the whole grating. Therefore, it is necessary to analyze the tolerance range of these parameters. Fig. 4 describes the comparison of grating period and transmission efficiency between FEM and RCWA under optimized parameters. We can see that when the grating period is set to 1007 nm, the transmission efficiency of the grating is the best value. In the range of 947 nm - 1035 nm, the transmission efficiency of TE and TM polarization at ± 1 st still reaches

more than 48%. Fig. 5 shows the comparison of duty cycle and transmission efficiency of FEM and RCWA under optimized parameters. For TE and TM polarization, when the duty cycle f is in the range of 0.3-0.4, the transmission efficiency of ± 1 st is more than 45%, and the suppression effect for 0th is more than 90%. Fig. 6 shows the comparison of incident angle and diffraction efficiency between the two methods under optimized parameters. In the angle range of -4° to 4° , the transmission efficiency of TE polarization is more than 40%, and the transmission efficiency of TM polarization is still more than 45%. In a word, the larger tolerance range enables the grating to effectively reduce the performance deviation caused by processing errors, thus maintaining efficient and stable optical performance.

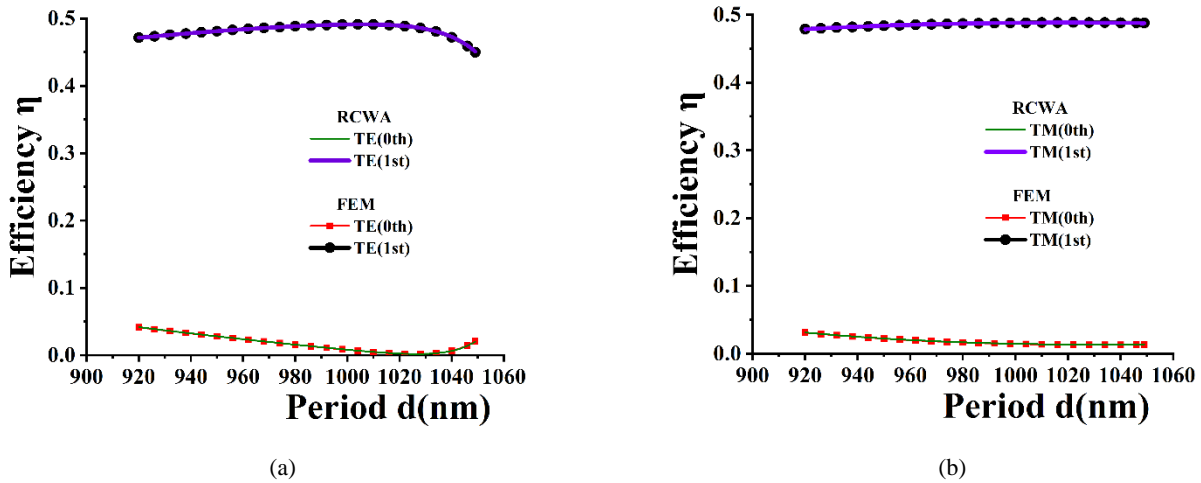


Fig. 4. Diffraction efficiency at different period under normal incidence with incident wavelength $\lambda=800$ nm, duty cycle $f=0.38$, $h_1=0.15$ μm , $h_2=0.31$ μm : (a) TE polarization, (b) TM polarization (color online)

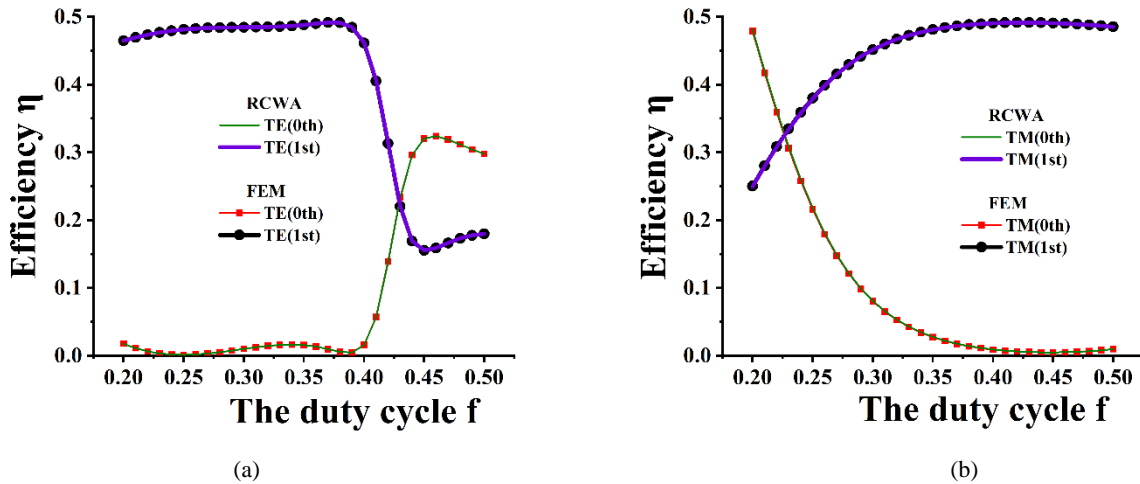


Fig. 5. Diffraction efficiency at a range of duty cycle under normal incidence with incident wavelength $\lambda=800$ nm, period $d=1007$ nm, $h_1=0.15$ μm , $h_2=0.31$ μm : (a) TE polarization, (b) TM polarization (color online)

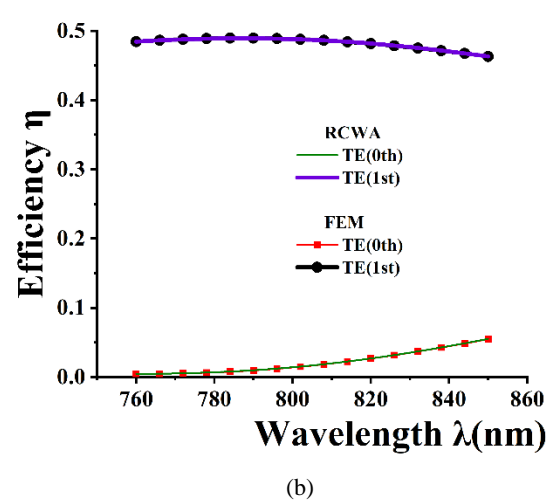
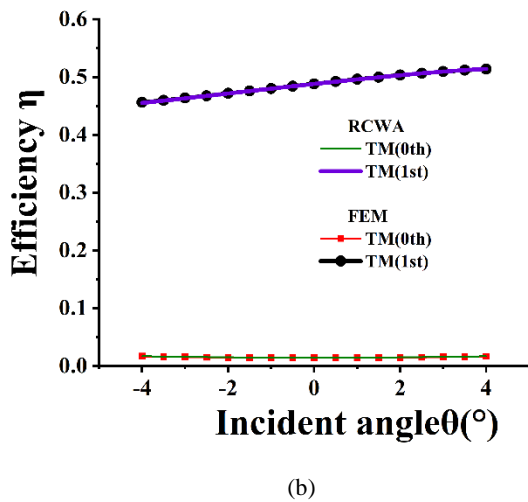
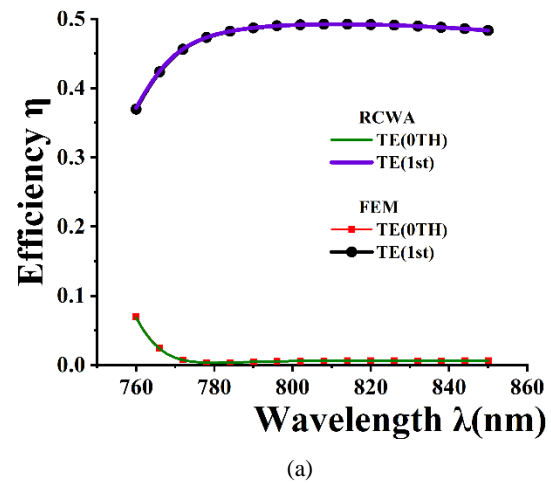
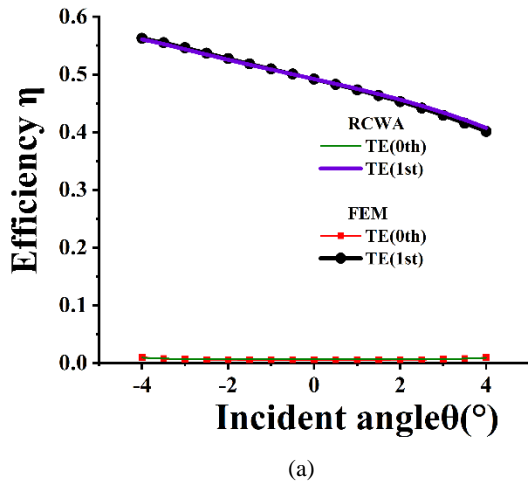


Fig. 6. Diffraction efficiency at a range of incident angle under normal incidence with incident wavelength $\lambda=800$ nm, period $d=1007$ nm, $h_1=0.15$ μm , $h_2=0.31$ μm , duty cycle $f=0.38$:
(a) TE polarization, (b) TM polarization (color online)

Fig. 7. The relationship between transmission efficiency and incident wavelength under normal incidence with $d=1007$ nm, $f=0.38$, $h_1=0.15$ μm and $h_2=0.31$ μm : (a) TE polarization, (b) TM polarization (color online)

In practical applications, bandwidth is also one of the important standards to measure the performance of gratings. One of the advantages of the beam splitter introduced in this paper is its excellent bandwidth. Fig. 6 shows the comparison of the relationship between incident wavelength and transmission efficiency of FEM and RCWA under the optimized parameters. When the incident wavelength is 800 nm and the normal incident, the transmission efficiency of the grating is in the best state. When the wavelength is in the range of 777 nm to 840 nm, for TE and TM polarization, the diffraction efficiency of the grating at $\pm 1\text{st}$ still exceeds 47%, and it maintains excellent zero order suppression performance. This wide bandwidth characteristic is of great significance for the practical application of the grating.

4. Conclusion

In this paper, a two-port transmission grating with a two-layer array sandwich structure is introduced. By using RCWA and simulated annealing algorithm to analyze and optimize the structure and parameters of the grating, not only can the grating achieve high transmission efficiency of $\pm 1\text{st}$ under TE and TM polarization, but also shows excellent 0th suppression characteristics. For TE and TM polarization, the transmission efficiency of $\pm 1\text{st}$ is 49.12% and 48.83% respectively, and the efficiency of 0th is 0.56% and 1.4% respectively. In addition, the accuracy of the results is ensured through the verification of FEM. Through analysis, it is found that the grating mentioned not only has good manufacturing tolerance, but also has the characteristics of wide bandwidth. Therefore, this kind of optical element with high efficiency and stable

performance plays an important role in the application of optical field.

Acknowledgements

This work is supported by the Science and Technology Program of Guangzhou (202002030284, 202007010001).

References

- [1] K. Zelaya, V. Hussin, O. Rosas-Ortiz, *Eur. Phys. J. Plus* **136**(5), 534 (2021).
- [2] V. G. Gurzadyan, A. T. Margaryan, *Eur. Phys. J. Plus* **136**(3), 329 (2021).
- [3] Z. Lin, B. Wang, Z. Huang, *Eur. Phys. J. Plus* **137**(9), 1094 (2022).
- [4] Y. Sun, L. Zhang, H. Xia, S. Cao, L. Wang, S. Yang, Y. Wu, R. Tai, *Optik* **227**, 166096 (2021).
- [5] S. An, J. Lv, Z. Yi, C. Liu, L. Yang, F. Wang, Q. Liu, W. Su, X. Li, T. Sun, P. K. Chu, *Optik* **226**, 165779 (2021).
- [6] H. Ni, L. Zhang, A. Ping, A. V. Krasavin, H. Ali, B. Ni, J. Chang, *Opt. Express* **30**(4), 5758 (2022).
- [7] D. Sang, M. Xu, Q. An, Y. Fu, *Opt. Express* **30**(15), 26664 (2022).
- [8] A. K. Sharma, A. K. Pandey, *IEEE Sens. J.* **20**(3), 1275 (2020).
- [9] T. Wang, S. S. Ng, *Optik* **262**, 169338 (2022).
- [10] P. Yuan, S. Weng, S. Ji, D. Zhang, L. Zhu, *Opt. Eng.* **60**(6), 066101 (2021).
- [11] C. Li, D. Tang, J. Liao, W. Wang, R. Dai, *Opt. Eng.* **61**(2), 026105 (2022).
- [12] Q. Pan, S. Zhou, Y. Guo, Y. Shuai, *Optik* **259**, 169031 (2022).
- [13] D. Shao, R. Zhang, Z. Fu, X. Guo, S. Zhuang, J. C. Cao, *Semi. Sci. Tech.* **34**(7), 075029 (2019).
- [14] A. M. Hammond, J. B. Slaby, M. J. Probst, S. E. Ralph, *Opt. Express* **30**(17), 31058 (2022).
- [15] D. Hu, Y. Zhang, Y. Zhao, X. Duan, *Opt. Express* **30**(2) 2131 (2022).
- [16] X. Mu, Z. Chen, L. Cheng, S. Wu, A. Pepe, X. Tu, H. Y. Fu, *Opt. Commun.* **482**, 126562 (2021).
- [17] Q. Sun, H. Chen, T. Wang, J. Wang, J. Yang, H. Jia, *Opt. Commun.* **522**, 128665 (2022).
- [18] Z. Xiong, B. Wang, X. Zhu, Y. Huang, L. Li, J. Hong, Y. Zhou, *Optoelectron. Adv. Mat.* **16**, 187 (2022).
- [19] X. Zhu, B. Wang, Z. Xiong, Y. Huang, *Optik* **260**, 169049 (2022).
- [20] Q. Liu, Z. Wang, L. Zhu, X. Cheng, J. Wang, *Opt. Laser Technol.* **138**, 106842 (2021).
- [21] J. Buencuerpo, J. M. Llorens, J. M. Ripalda, M. A. Steiner, A. C. Tamboli, *Opt. Laser Technol.* **142**, 107224 (2021).
- [22] Z. Lin, B. Wang, C. Fu, *Phys. Scr.* **96**(12), 125540 (2021).
- [23] S. K. Dubey, A. Kumar, A. Kumar, A. Pathak, S. K. Srivastava, *Optik* **252**, 168527 (2022).
- [24] S. Golharani, B. Jazi, E. Heidari-Semiromi, Z. Rahmani, *Optik* **241**, 167257 (2021).
- [25] J. Li, J. Chen, X. Liu, H. Tian, J. Wang, J. Cui, S. Rohimah, *Appl. Opt.* **60**(18), 5312 (2021).
- [26] Y. Zhou, X. Li, B. Wang, L. Li, *Optik* **259**, 169014 (2022).
- [27] J. Wang, C. Zhou, J. Ma, Y. Zong, W. Jia, *Appl. Opt.* **55**(19), 5203 (2016).
- [28] H. Cao, J. Wu, J. Yu, J. Ma, *Appl. Opt.* **57**(4), 900 (2018).
- [29] J. Feng, C. Zhou, H. Cao, P. Lu, *Appl. Opt.* **49**(30), 5697 (2010).
- [30] Z. Lin, B. Wang, K. Wen, *Opt. Commun.* **505**, 127499 (2022).
- [31] H. Situ, Z. He, *Eur. Phys. J. Plus* **137**(1), 98 (2022).
- [32] M. Jamei, I. Ahmadianfar, M. Jamei, M. Karbasi, A. A. Heidari, H. Chen, *Eur. Phys. J. Plus* **137**(3), 289 (2022).
- [33] M. Ou, L. Liu, Y. Liu, L. Lan, S. Xie, X. Shi, *Optik* **225**, 165722 (2021).
- [34] S. Zhou, H. Xie, C. Zhang, Y. Hua, W. Zhang, Q. Chen, G. Gu, X. Sui, *Optik* **244**, 167516 (2021).

*Corresponding author: wangb_wsx@yeah.net